ISSN PRINT 2319 1775 Online 2320 7876

Research paper UGC CARE Listed (Group -I) Journal Volume 11, Iss 12, Dec 2022

STRUCTURAL AND MAGNETIC PROPERTIES OF NANOCRYSTALLINE $SrFe_{12}O_{19}$ HEXAFERRITES PREPARED BY AUTO COMBUSTION METHOD USING MIXED FUELS

Usharani*

[a]Department of Mathematics, Sri Datta Arts, Commerce and Science, Degree College, Kalaburagi-585 101, Karnataka, India

Email address: *usharanichavan7@gmail.com*

ABSTRACT

The nanocrystalline $Sr_{(1-x)}Ce_xFe_{12}O_{19}$ (x = 0.0, 0.01, 0.3, 0.05, 0.07 and 0.09) M-type hexaferrites have been prepared via auto combustion using mixed fuels. The morphology and compositions were analysed using XRD, FT-IR and FE-SEM techniques. XRD peaks revealed the nanocrystalline nature of the samples having single phase magnetoplumbhite-type hexagonal crystal structure. Strong absorption FT-IR bands observed in range 300 - 1000 cm^{-1} and the force constant of tetrahedral site is less than octahedral site which shows Ce^{3+} occupies Sr^{2+} sites. The FESEM micrographs exhibit the compact magnetic piled up aggregation of nano hexaferrite. The particle size decreased with increase in Ce^{3+} ion content. The magnetic properties by VSM studies confirmed the hard nature of strontium ferrite with increase in Ce^{3+} content. It was found that saturation magnetization and magnetic parameters of strontium ferrites decreases with increase of Ce^{3+} content. Nano-hexaferrites are useful for magnetic recording and memory devices.

Keywords: Hexaferrites, Hard ferrites, Magnetic Properties, Auto combustion method.

INTRODUCTION

Ferrites are mixed metal oxides with iron oxides as their major component with the general formula AB_2O_4. Nanocrystalline ferrites contribute major part in the fabrication of magnetic materials due to their novel physical properties and high frequency devices, magnetic recording media, catalysis, transformer cores, radiation and absorption devices, medical diagnostics, ferro fluids and biomedical fields [1-3]. M-type hexaferrites have

ISSN PRINT 2319 1775 Online 2320 7876

Research paper UGC CARE Listed (Group -I) Journal Volume 11, Iss 12, Dec 2022

chemical formula $MFe_{12}O_{19}$, where M may be Barium (Ba), Strontium (Sr) or Lead (Pb) [3]. M-type hexaferrites are important materials have high chemical stability, specific saturation magnetization, uniaxial magneto crystalline anisotropy, coercivity, high Curie temperature and electrical resistivity along with low dielectric losses [4-6]. Nanostructured hexaferrites have received much attention owing to technological and industrial applications that lend use as permanent magnets [7]. The intrinsic properties of $SrFe_{12}O_{19}$ were greatly affected by the both synthesis method and cationic exchange [8]. Strontium M-type hexaferrites are found demanding and competitive application with changing technology, the most commonly used materials for the permanent ferrite magnets [9] for which there is massive demand from manufacturers of microwave devices, magnetic recording media, telecommunications devices, and so on [10]. Doping strontium hexaferrite with transition metal ion or rare earth ions of comparable size has resulted in a considerable change in its properties [11, 12]. Magnetic properties of substituted magnetic nanoferrites depend on both types and concentration of doped element, morphology, particle size and the approach of synthesis [13, 14]. Substitution of small amount of rare earth elements into strontium hexaferrites lead to the significant modification in their electrical and magnetic properties [8, 11]. Many researcher have studied rare earth substituted for strontium hexaferrites and reported significant changes in magnetic properties [15], such as La^{3+} [16] Ce^{3+} [17], Pr^{3+} [18], Nd^{3+} [19], Sm^{3+} [20], Gd^{3+} [21]. The properties of this magnetic material depend on the purity, size and morphology of the precursor powder [22]. Thus obtaining fine, high chemical homogeneity and monodispersed particles is the most important process in material manufacturing [22]. The improvement in magnetic properties of M-type hexaferrites with substitution of rare earth ions are explained as increase in magneto crystalline anisotropy and coercive field with magnetization [23]. Nowadays, hexaferrites are being used in electric power generation, nanocatalyst, microwave absorber, automotive electronics, rotors in small DC motors microwave devices and ferrite cores. Various preparation techniques have been used to synthesize strontium hexaferrite including hydrothermal method [24], sono chemical method [25], reverse micelle technique [26], micro-emulsion [27], combustion routes [28] co-precipitation [29] and sol-gel [30]. The auto combustion method involves simplicity, low cost, highest crystallinity and purity, good chemical homogeneity, low processing time, and fine distribution of particles size [31].

ISSN PRINT 2319 1775 Online 2320 7876

Research paper UGC CARE Listed (Group -I) Journal Volume 11, Iss 12, Dec 2022

From the literature survey, no reports have been found regarding the synthesis of strontium hexaferrites by auto combustion method by using mixed fuels. Therefore, we have investigated the influence of Ce^{3+} ion substitution on the structural and magnetic properties of nanocrystalline $Sr_{(1-x)}Ce_xFe_{12}O_{19}$ (x = 0.0, 0.01, 0.3, 0.05, 0.07 and 0.09) hexaferrites prepared via auto combustion using mixed fuels.

EXPERIMENTAL METHOD

In present investigation, the auto combustion with mixed fuels synthesis technique was successfully used to synthesize $Sr_{(1-x)}Ce_xFe_{12}O_{19}$ (with x = 0, 0.01, 0.03, 0.05, 0.07 and 0.09) nanoferrites using analytical reagent grade Strontium nitrate ($Sr(NO_3)_2$) [Merck], ferric nitrate ($Fe(NO_3)_3.9H_2O$), cerium nitrate ($Ce(NO_3)_3.6H_2O$) [Sigma Aldrich], glycine [$C_2H_5NO_2$] and urea [CH_4N_2O]. Stoichiometric ratios of reactants with fuels are dissolved in de-ionized water. The aqueous solution containing redox mixture was taken in a Pyrex dish and heated in a muffle furnace maintained at 500 ± 10ºC in air atmosphere. Initially, the solution boils in a muffle furnace and undergoes dehydration followed by decomposition with the evolution of large amount of gases (N_2O and CO_2). The combustion propagates throughout the reaction mixture without further need of any external heating, as the heat of the reaction is sufficient for the decomposition of the redox mixture. The type of combustion is smoldering in nature and reaction time of the actual ignition was 16-18s. These gases are known to be hypergolic. This result in better homogenization of the product by bringing close together the unreacted particles that tends to reduce diffusion distances as well as grain size distribution. At this stage, pristine powders were ground in agate mortar and mixed with a binder. The powders were ground into fine powder and further calcinated at 1000 °C for 3 hours. The powders are compressed into pellets of 10 mm in dia and ~2-3 mm in thickness by loading a pressure of 5-10^8 kg/m^2 for 5 minutes. Further, the pellets are sintered at temperature, 1100 °C for 20h in furnace and then gradually cooled up to room temperature. The purity set of samples obtained due to result of auto combustion process with mixed fuel which involves rapid exothermic reaction between glycine, urea and metal nitrates.

CHARACTERIZATION

The X-ray diffraction patterns of nanoferrites have been recorded on X-ray diffractometer (Make: Bruker, Model: D8 Advance, Germany) with CuKα radiation bearing

ISSN PRINT 2319 1775 Online 2320 7876

Research paper UGC CARE Listed (Group -I) Journal Volume 11, Iss 12, Dec 2022

wavelength 1.5406 A^0, in Bragg angle, 2θ, range from 20^0 - 80^0 at the chart speed of 2^0/ min at 300K. Room temperature FTIR spectra of all nanoferrites were recorded by employing Thermo-Nicolet 6700 Fourier transform infrared spectrometer (Make: Perkin Elmer, Model: Spectrum Two, USA) in the wavenumber range 4000-300cm^{-1}. The samples (0.5mg to 1.0 mg) were mixed with spectral grade potassium bromide (KBr) as the standard ground and then pressed to obtain circular discs of appropriate 1mm thickness. The micrographs of sintered pellets and composition analysis of all the samples investigated in the present investigation were obtained by employing (FESEM, JEOL/EO JSM—639; EDS Make: Carl Zeiss, Model: EVOLSI5, Germany. The saturation magnetization-Ms, remanent magnetization-Mr and coercivity-Hc of all nanoferrites were measured at 300K using vibrating sample magneto meter (Make: Crest, Model: 20130523-01).

RESULTS AND DISUSSION

X-ray diffraction analysis

The XRD powder patterns for $Sr_{(1-x)}Ce_xFe_{12}O_{19}$ (x=0, 0.01, 0.03, 0.05, 0.07 and 0.09) nano ferrites are depicted in **Fig 1.** From the analysis of XRD patterns, it is found that peaks with (hkl) values [planes] (110), (008), (107), (114), (201), (203), (205), (206), (217), (304) and (220) are tallied with JCPDS card number: 84- 1531 for M-type Strontium hexaferrites with hexagonal phase. Moreover, it is observed that the x = 0.09 sample shown about 5% of secondary phase of CeO_2 (JCPDS: 80-2377) [32]. The lattice parameter is calculated using the relation.

$$\frac{1}{d_{hkl}^2} = \frac{4}{3}\left[\frac{h^2 + hk + k^2}{a^2} + \frac{l^2}{c^2}\right] \dots\dots\dots (1)$$

where d_{hkl} is an interplanar spacing of the crystal; a and c are the lattice parameters; and (h k l) are the Miller indices. From the XRD studies it was found that the lattice parameter slightly increase (from 0.58796-0.58847 nm) with increasing the Ce^{3+} ion concentration due to replacement of larger ionic radius Sr^{2+} ions (0.112 nm) by smaller ionic radius Ce^{3+} ions (0.1034 nm) [32].

Unit cell volume (V_{cell}) of the hexagonal system is calculated as follows:

$$V_{cell} = 0.866\, a^2 c \dots\dots\dots (2)$$

Where, numeric factor is constant for the hexagonal system.

ISSN PRINT 2319 1775 Online 2320 7876

Research paper UGC CARE Listed (Group -I) Journal Volume 11, Iss 12, Dec 2022

From XRD profile, an average crystallites size of nanoferrites was determined using Debye-Scherer equation (d) is calculated by the Scherrer formula (3):

$$d = \frac{k\lambda}{\beta \cos\theta} \dots\dots\dots (3)$$

Where, k = 0.89 is Scherrer constant (the shape factor) for hexagonal system, λ=0.15406 nm is the wavelength of incident X-rays, β is the full width at half maximum of diffraction peak, θ is the Bragg angle of diffraction. It is found that an average value of crystallite size is in the range of 42-46 nm. The values are tabulated in the Table.1

The theoretical x-ray density (dx) of each sample was calculated using the formula

$$d_x = \frac{ZM}{NV} \dots\dots\dots (4)$$

Where Z= 2, is Number of molecules per unit cell, M is the molecular weight, N is the Avogadro's number and V is the volume of the unit cell.

Figure-1: XRD patterns of $Sr_{(1-x)}Ce_xFe_{12}O_{19}$ (x = 0.0, 0.01, 0.3, 0.5, 0.07, 0.09) nanoferrites

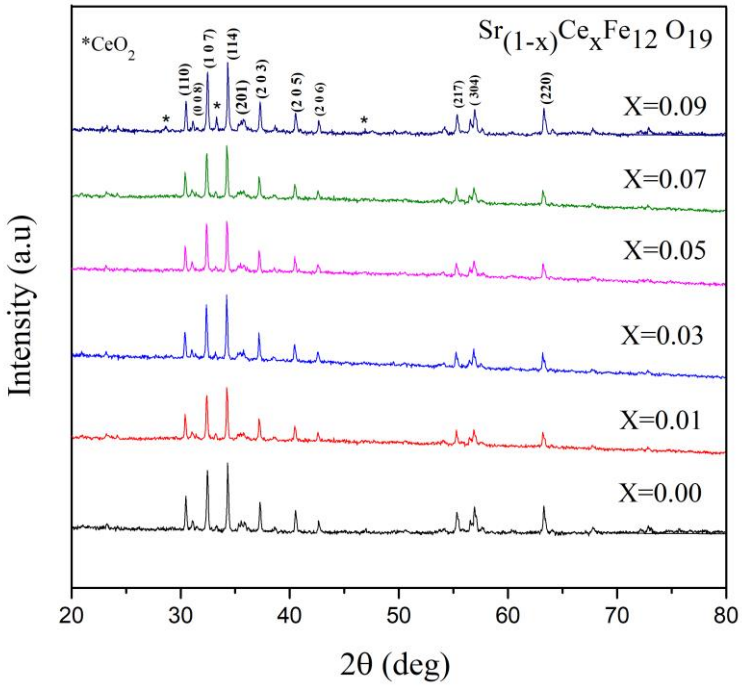

The cell volume V of the SrM phase was also determined and the different a, c and V parameters are listed in **Table 1.** The values of x-ray density are in the range of 4.73-5.11 g cm^{-3}. The decrease increase in the X-ray density is due greater molecular weight

ISSN PRINT 2319 1775 Online 2320 7876

Research paper UGC CARE Listed (Group -I) Journal Volume 11, Iss 12, Dec 2022

(140.116 u) and ionic volume (0.1034 nm) of Ce^{3+} ion than smaller molecular weight (87.62 amu) and larger ionic radius (0.112 nm) of strontium ions.

Table 1: Crystallite size (D), lattice constant (a & c), cell volume (V) and X-ray density (qx-ray) of $Sr_{(1-x)}Ce_xFe_{12}O_{19}$ (x=0.00, 0.01, 0.03, 0.05, 0.07 and 0.09) nanoferrites.

Composition	Crystallite size (D) /nm	Lattice constant (a)/Å	Lattice constant (c)/Å	(c)/(a) Å	Cell volume (V)/Å^3	X-ray density (qx-ray)/g cm^{-3}
$SrFe_{12}O_{19}$	45.54	5.8847	23.0552	3.918	691.4	5.10
$Sr_{0.09}Ce_{0.01}Fe_{12}O_{19}$	43.54	5.8796	23.0493	3.920	690.0	4.73
$Sr_{0.07}Ce_{0.03}Fe_{12}O_{19}$	42.25	5.8809	23.0475	3.919	690.3	4.74
$Sr_{0.05}Ce_{0.05}Fe_{12}O_{19}$	43.84	5.8823	23.0493	3.918	690.7	4.74
$Sr_{0.03}Ce_{0.07}Fe_{12}O_{19}$	43.53	5.8835	23.0518	3.918	691.0	4.74
$Sr_{0.01}Ce_{0.09}Fe_{12}O_{19}$	42.86	5.8828	23.0534	3.919	690.9	4.75

Spectral analysis

Represented the FT-IR spectrum of $Sr_{(1-x)}Ce_xFe_{12}O_{19}$ (x=0, 0.01, 0.03, 0.05, 0.07 and 0.09) nanohexaferrites. FTIR gives the information about molecular bond and chemical structure in the materials to confirm the formation of the single phase of doped and undoped ferrites For hexaferrites there are two strong characteristic absorption bands in the range between 300 and 1000 cm^{-1}, which are attributed to the intrinsic vibrations of tetrahedral and octahedral sites in the hexagonal lattice [34]. Band in the range 409-411 cm^{-1} corresponds to tetrahedral band, and band in the range 309–311 cm^{-1} corresponds to octahedral band. This confirms the formation of M-type hexaferrite structure. This shift is attributed to the variation of the Fe^{3+}–O^{2-} distances affected by substitution. These observations confirmed the formation of M-type hexaferrite structure. Non-appearance of any absorption band in the region 3200–3500 cm^{-1} reveals the absence of OH group/moister in the synthesized samples and hence confirms the completion of reaction [12, ….].

$$K_T = 4\pi^2 c^2 \upsilon_1^2 m \dots\dots\dots (4)$$

$$K_O = 4\pi^2 c^2 \upsilon_2^2 m \dots\dots\dots (5)$$

ISSN PRINT 2319 1775 Online 2320 7876

Research paper UGC CARE Listed (Group -I) Journal Volume 11, Iss 12, Dec 2022

Where c is velocity of light 2.99×10^{8} m/s, ν_1 and ν_2 are the vibrational frequencies at A- sites and B- sites, m is reduced mass of Fe^{3+} and O^{2-} ions (2.061×10^{-23} g).

From the table 2, it is observed that K_T values are lower than K_O. Further, the K_T and K_O values of are significance constant with increase in Ce^{3+} ion content.

A force constant is a second derivative of potential energy related to the site radius. It is observed that K_T is higher K_O. Further, the K_T values of are found almost constant with increase in Ce^{3+} content. However, K_O values are less than K_T values in Ce^{3+} ions substituted samples as shown.

Table 2: Position of IR absorption bands and force constant of $Sr_{(1-x)}Ce_xFe_{12}O_{19}$ (*x*=0.00, 0.01, 0.03, 0.05, 0.07 and 0.09) nanoferrites.

Composition	Position of ν_1(cm^{-1})	Force Constant Tetrahedral (K_T) dynes/cm	Position of ν_2 (cm^{-1})	Force Constant Octahedral (K_O) dynes/cm
$SrFe_{12}O_{19}$	310	701	411	1231
$Sr_{0.09}Ce_{0.01}Fe_{12}O_{19}$	311	705	410	1225
$Sr_{0.07}Ce_{0.03}Fe_{12}O_{19}$	309	696	411	1231
$Sr_{0.05}Ce_{0.05}Fe_{12}O_{19}$	309	696	411	1231
$Sr_{0.03}Ce_{0.07}Fe_{12}O_{19}$	310	701	409	1219
$Sr_{0.01}Ce_{0.09}Fe_{12}O_{19}$	311	705	409	1219

Morphological studies

The FE-SEM images of the synthesized compositions $Sr_{(1-x)}Ce_xFe_{12}O_{19}$ (**x = 0.0, 0.1 and 0.9**) have shown in **Fig. 2(a-c).** From the Fig. 2(a), it is observed that the grains are grown in the compact magnetic piled up aggregation for the $SrFe_{12}O_{19}$ nanoferrites. These hexaferrite particles due to its magnetic nature and the union of primary particles held together by weak (van der Waals forces) surface interaction. Moreover, the samples are extremely porous in nature. The grain sizes are in the range of 42-46 nm. These values are in consistent with values calculated from XRD. **Fig. 2(b-c)** revealed the hexagonal shape morphology of the strontium hexaferrite derivatives. Further, it is evident that the extremely fine powders show

ISSN PRINT 2319 1775 Online 2320 7876

Research paper UGC CARE Listed (Group -I) Journal Volume 11, Iss 12, Dec 2022

a strong tendency to formation of aggregates into large cluster. The reports indicated that the auto-combustion method with mixed fuel reaction involves crystallization formation as compared to the crystal from a solution of hexaferrite nanoparticles, due to extended time span and high temperature for the completion of auto-combustion method with mixed fuel sovereign to the variant particle size distribution.

Figure-2: FESEM Micrographs of $Sr_{(1-x)}Ce_xFe_{12}O_{19}$ (x = 0.0 (a), 0.01(b) and 0.09(c)) nanoferrites

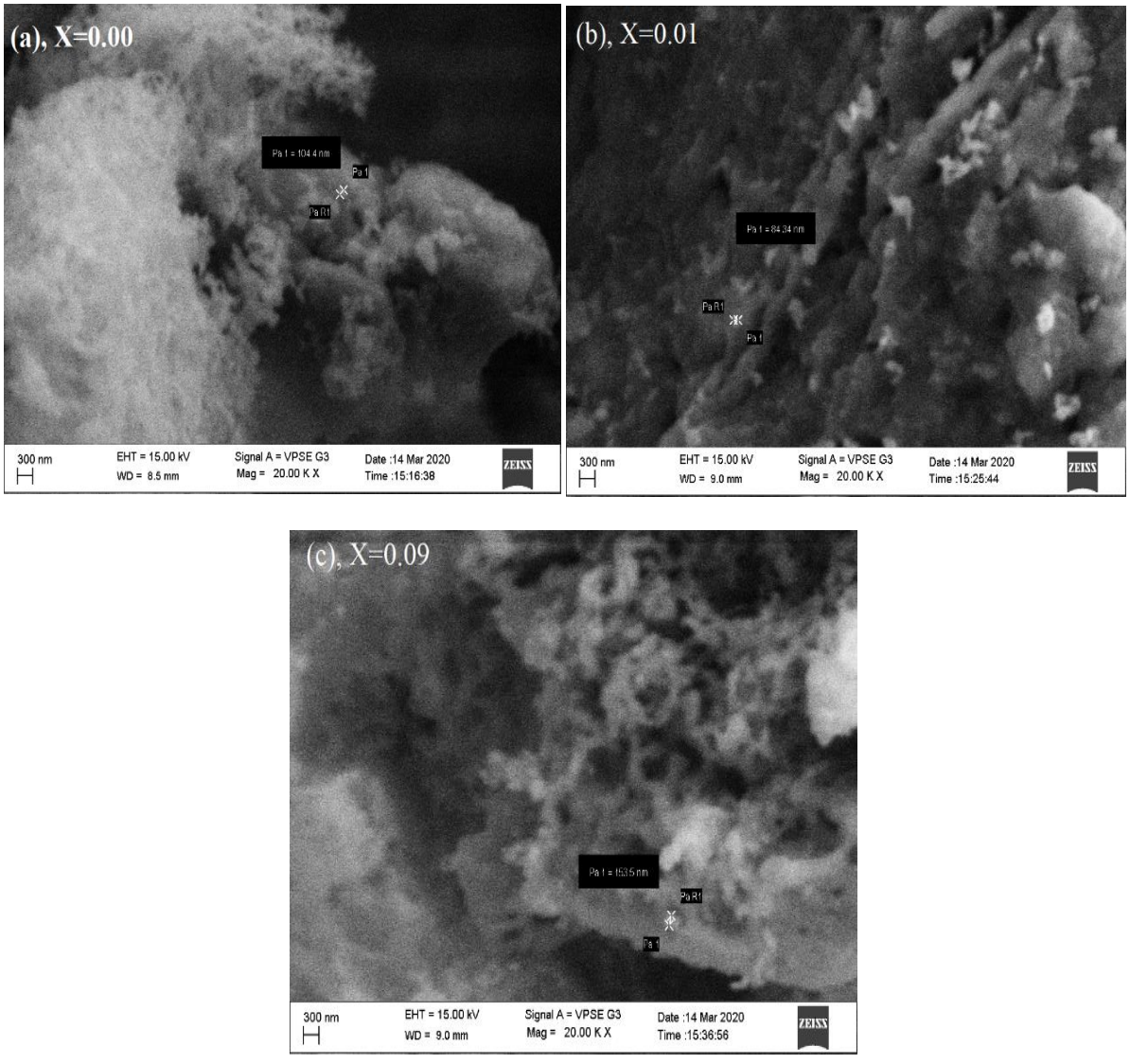

Magnetic properties

The variations of Saturation magnetization (Ms), coercive field (Hc), remanence magnetization (Mr), and squareness ratio (Mr/Ms) of $Sr_{(1-x)}Ce_xFe_{12}O_{19}$ (x = 0, 0.01, 0.03, 0.05, 0.07 and 0.09) nanohexaferrites with at room temperature is shown figure-3. The magnetic parameters were calculated using the following relations

ISSN PRINT 2319 1775 Online 2320 7876

Research paper UGC CARE Listed (Group -I) Journal Volume 11, Iss 12, Dec 2022

$$n_B = \frac{M \times M_S}{5585} \ldots\ldots\ldots (6)$$

$$S = \frac{M_r}{M_s} \ldots\ldots\ldots (7)$$

$$K = \frac{H_C \times M_S}{0.64} \ldots\ldots\ldots (8)$$

Where n_B is the magnetic moment / formula unit in μ_B, M_s is saturation magnetization (emu/g), M_r is the remanent magnetisation, M is the molecular weight in g, 5585 is the magnetic factor, k is the magnetic anisotropic constant and Hc is the coercivity. The Yafet and Kittel angles are given by the relation

$$\text{Cos } \alpha(Y-K) = \left[\frac{n_B + 5(1-x)}{(6-x)}\right] \ldots\ldots\ldots (9)$$

Fig 3, the magnetic hysteresis loops revealed that the synthesized nanohexaferrites exhibit ferrimagnetic and hard magnetic nature behaviour. Moreover, the saturation magnetisation (M_S) and remnant (M_r) magnetizations, the coercive (H_C) and magneto-crystalline anisotropy (K) fields are decreased with increase in the Ce^{3+} ion concentration. The H_C values are very high, pointing to the hard ferrimagnetic characteristics of the nanohexaferrites. Further, it is found that M_r/M_S, values are almost constant for all nanohexaferrites.The values of Ms, Mr, Hc, (Mr/Ms), n_B, K and Y-K angles are tabulated in figure-3

Figure-3: Hysteresis curves of $Sr_{(1-x)}Ce_xFe_{12}O_{19}$ (x = 0.0, 0.01, 0.3, 0.5, 0.07, 0.09) nanoferrites

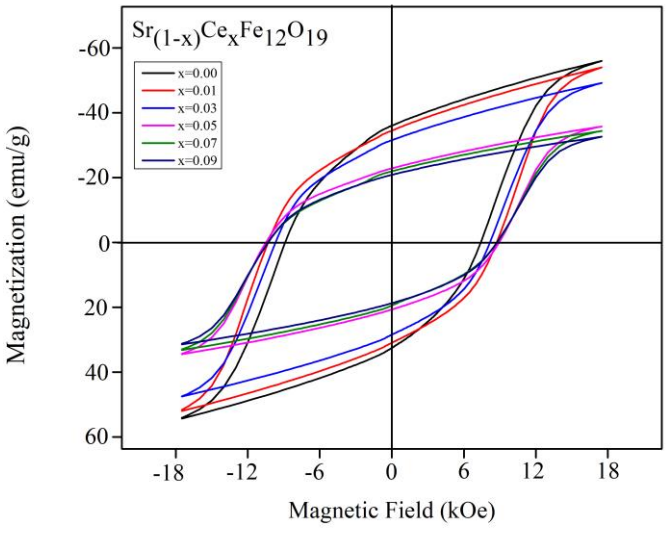

ISSN PRINT 2319 1775 Online 2320 7876

Research paper UGC CARE Listed (Group -I) Journal Volume 11, Iss 12, Dec 2022

The magnetic moment of Sr-hexaferrites is originated from Fe^{3+} ions that occupy the five different sub-lattices. Therefore, Fe^{3+} ions in the 12k, 2a and 2b sites exhibit spins-up, however, those in the $4f_1$ and $4f_2$ sites exhibit spins-down. Therefore, the net magnetic moment is equal to the difference between the magnetic moments with spin-up and spin-down. According to Neel, the calculated magneton number is given by $M_S = M_B - M_A$ where, M_B is the magnetic moment of B site (octahedral) cation and M_A is a magnetic moment of A site (tetrahedral) cation. In order to calculate M_B and M_A the probable cation distribution of the present system, M decreases with the B-site replacements. The substituting Fe^{3+} ions preferably occupied the B-site. Note that the magnetic moment of Ce^{3+} ions is larger than that of Fe^{3+} ions. When the number of Fe^{3+}-O-Fe^{3+} super exchange interactions of ions at B-site decreased, the magnetization of B-sublattice decreased. However, if the substituting ions substitute by the Fe^{3+} ions in the down spins sites, the net magnetic moment increases [12], The magnetic moment of strontium ion was decreases with increasing Ce^{3+} ion, this action to be for the increase in values is resulting from the reinforcement of the super exchange interactions among various sites lead to an increase in values (13.77 – 8.33 μB). This indicates a reinforcement of the super-exchange interactions. The magnetisation values of $SrFe_{12}O_{19}$ samples are reduce from for Ms 72.18 emu/g - 43.81 emu/g with increase in Ce^{3+} ion content [17, 42]. The Mr in the range 44.7 4- 27.06 emu/g at room temperature. Hc is in the range of 9786 - 8146 Oe at room temperature. This reduction is attributed to an equivalent reduction of Fe^{3+} ions to Fe^{2+} ions for charge compensation in substitution of Ce^{3+} ions instead of Sr^{2+} ions. Moreover, the magnetic moment of Fe^{2+} ions (4 μB) is less than that in Fe^{3+} ions (5 μB) [12]..

Y-K-Yafet-Kittel angle, the degree of spin canting effect is explained with the help of Yafet- Kittle angle (αY-K). The calculated values of α (Y-K) are found to be decrease from 15 – 9 degree increase in Ce^{3+} ion concentration owing to molecular field approximation using a non-collinear three sub-lattice model and an increasing tendency for triangular spin arrangement exchange interaction.

Conclusions

Nanocrystalline $Sr_{(1-x)}Ce_xFe_{12}O_{19}$ (x = 0.0, 0.01, 0.3, 0.05, 0.07 and 0.09) hexaferrites were synthesized by auto combustion method using mixed fuels. X-ray diffraction studies confirmed the single magneto-plumbite hexagonal phase of all the samples. The FT-IR

ISSN PRINT 2319 1775 Online 2320 7876

Research paper UGC CARE Listed (Group -I) Journal Volume 11, Iss 12, Dec 2022

spectrum shows the two absorption bands which are the characteristics bands of nanoferrites. The FESEM studies confirmed that the morphological structure was agglomerated with nano particle sizes. The magnetic parameter decreases with increasing the Cerium ion concentration. The synthesised hexaferrites exhibit hard magnetic nature. The different exchange paths between the iron sub-lattices are discussed according to the increased hyperfine fields. Thus, the subsequent tuning of the Ce^{3+} in $SrFe_{12}O_{19}$ confirms the use of $SrFe_{12}O_{19}$ in applications like magnetic recording, memory devices, construction of permanent magnet which is used in transformers, generators, motors and galvanometers etc.

Acknowledgement

Thankful for supporting the magnetic measurements were performed at Indian Institute Science. Bangalore.

REFERENCEES

[1] K. K. Mallick, Philip Shepherd, R.J. Green, Dielectric properties of M-type barium hexaferrite prepared by co-precipitation, J. Eur. Ceram. Soc. 27 **(2007)**

[2] A. Goldman, Modern Ferrite Technology II, Springer Science Inc., USA, **(2006)** 63.

[3] A. Liaquat, M. Anis-ur-Rehman, A. ul Haq, Impact of Gd doping on the dielectric and magnetic properties of (Sr-Ba) $Fe_{12}O_{19}$ nanoparticles, J. Alloys Comp 822 **(2020)** 15.

[4] M.A. Almessiere, Y. Slimani, H. Güngüneş, H.S. El Sayed, A. Baykal, AC susceptibility and Mossbauer study of Ce^{3+} ion substituted $SrFe_{12}O_{19}$ Nanohexaferrites, Ceram. Int, 44(9) **(2018)** 10470-10477.

[5] R.A. Pawar, S.S. Desai, Q.Y. Tamboli, S. E. Shirsath, S.M. Patange, Ce^{3+} incorporated structural and magnetic properties of M type barium hexaferrites, J. Magn. Magn. Mater. 378 **(2015)** 59–63.

[6] A. Zafar, A. Rahman, S. Shahzada, S. Anwar, M. Khan, A. Nisar, M. Ahmad, S. Karim, Electrical and magnetic properties of nano-sized Eu doped barium hexaferrites, J. Alloy. Compd. 727 **(2017)** 683–690.

[7] K. Kamishima, T. Mashiko, K. Kakizaki, M. Sakai, K. Watanabe, H. Abe, Synthesis and magnetic characterization of Sr-based Ni_2X-type hexaferrite. AIP Adv.5 **(2015)** 107132.

[8] J. Töpfera, D. Seiferta, J.-M. Le Bretonb, F. Langenhorstc, V. Chland, K. Kourˇild, H. Šteˇpánková, J. Solid State Chem. 226 **(2015)** 133–141.

[9] R. C. Pullar, Hexagonal ferrites: a review of the synthesis, properties and applications of hexaferrite ceramics, Prog. Mater Sci. 57 **(2012)** 1191–1334.

[10] T. J. Pérez-Juache, A.L. Guerrero, J.G. Cabal-Velarde, M. Mirabal-García, S. A. Palomares-Sánchez, J.A. Matutes-Aquino, Analysis of the structure and Mossbauer study of the neodymium substitution in the Sr-hexaferrite, Phys. B 503 **(2016)** 183–188.

ISSN PRINT 2319 1775 Online 2320 7876

Research paper UGC CARE Listed (Group -I) Journal Volume 11, Iss 12, Dec 2022

[11] M. N. Ashiq, A. S. Asi, S. Farooq, M. Najam-ul-Haq and S. Rehman. Magnetic and electrical properties of M-type nano-strontium hexaferrite prepared by sol-gel combustion method. J. Magn. Magn. Mater. 444 **(2017)** 426–431 .

[12] M.A. Almessierea, Y. Slimani, H.S. El Sayed, A. Baykal, I. Ercan Microstructural and magnetic investigation of vanadium-substituted Sr nanohexaferrites, J. Magn. Magn. Mater. 471 **(2019)** 124–132.

[13] A. G. Abraham, A. Manikandan, E. Manikandan, S. Vadivel, S.K. Jaganathan, A. Baykal, P. Sri Renganathan, Enhanced magneto-optical and photo-catalytic properties of transition metal cobalt (Co^{2+} ions) doped spinel $MgFe_2O_4$ ferrite nanocomposites, J. Magn. Magn. Mater. 452 **(2018)** 380-388.

[14] E. Hema, A. Manikandan, M. Gayathri, M. Durka, S.A. Arul, B. R. Venkatraman, The Role of Mn^{2+}Doping on Structural, Morphological, Optical, Magnetic and Catalytic Properties of Spinel $ZnFe_2O_4$Nanoparticles, J. Nanosci and Nanotec 16 **(2016)** 5929-5943.

[15] Y. Li, Y. Huang, S. Qi, L. Niu, F. Niu, Y. Zhang, Y. Wu, Preparation and magnetic properties of Ce-doped strontium ferrite films, Adv. Mat. Res, 239-242 **(2011)** 481-485.

[16] D. Seifert, J. Töpfer, F. Langenhorst, J.-M. Le Breton, H. Chiron, L. Lechevallier, Synthesis and magnetic properties of La substituted M-type Sr hexaferrites. J. Magn. Magn. Mater. 321 **(2009)** 4045.

[17] Z. Mosleh, P. Kameli, A. Poorbaferani, M. Ranjbar, H. Salamati, Structural, magnetic and microwave absorption properties of Ce-doped barium hexaferrite. J. Magn. Magn. Mater. 397 **(2016**) 101.

[18] J. F. Wang, C. B. Ponton, I.R. Harris, A study of Pr-substituted strontium hexaferrite by hydrothermal synthesis, J. Alloy. Compd. 403 **(2005**) 104–109.

[19] B.H. Bhat, B. Want, Dielectric and impedance behavior of neodymium substituted strontium hexaferrite. Appl. Phys. A 122, 148 **(2016).**

[20] L. Lechevallier, J.M. Le Breton, A. Morel, J. Teillet, Structural and magnetic properties of $Sr_{1-x}Sm_xFe_{12}O19$ hexagonal ferrites synthesised by a ceramic process, J. Alloy. Compd. 359 **(2003**) 310–314.

[21] G. Litsardakis, I. Manolakis, C. Serletis, K.G. Efthimiadis, Effects of Gd substitution on the structural and magnetic properties of strontium hexaferrites, J. Magn. Magn. Mater. 316 **(2007)** 170–173.

[22] H. F. Lu, R.Y. Hong, H.Z. Li, Influence of surfactants on co-precipitation synthesis of strontium ferrite J. Alloys and Compd 509 **(2011)** 10127– 10131.

[23] D. Seifert, J. Töpfer, M. Stadelbauer, R. Grössinger, J.-M.L. Breton, Rare-Earth-Substituted $Sr_{1-x}Ln_xFe_{12}O_{19}$ Hexagonal Ferrites, Am. Ceram. Soc. 94 **(2011)** 2109.

[24] M. Sivakumar, A. Gedanken, W. Zhong, Y.W. Du, D. Bhattacharya, Y. Yeshurun, I. Felner, Nanophase formation of strontium hexaferrite fine powder by the sonochemical method using $Fe(CO)_5$, J. Magn. Magn. Mater. 268 (2004) 95–104.

[25] J. Fang, J.Wang, L.-M. Gan, S.-C. Ng, J. Ding, X. Liu, Fine Strontium Ferrite Powders From an ethanol-based micro emulsion J. Am. Ceram. Soc. 83 **(2000)** 1049–1055.

ISSN PRINT 2319 1775 Online 2320 7876

Research paper UGC CARE Listed (Group -I) Journal Volume 11, Iss 12, Dec 2022

[26] D. H. Chen, Y.Y. Chen, Synthesis of Strontium Ferrite Ultrafine Particles Using Microemulsion Processing J. Colloid Interface Sci. 236 **(2001)** 41–46.

[27] D.S. Mathew, R.S. Juang, An Overview of the Structure and Magnetism of Spinel Ferrite Nanoparticles and Their Synthesis in Microemulsion, Chem. Eng. J. 129 **(2007)** 51–65.

[28] Z.X. Yue, J. Zhou, L.T. Li, H.G. Zhang, Z.L. Gui, Synthesis of nanocrystallineNiCuZn ferrite powders by sol–gel auto-combustion method J. Magn. Magn. Mater. 208 **(2000)** 55–60.

[29] J.F. Crider, Self-Propagating high temperature synthesis - A Soviet method, for Producing Ceramic materials Ceram. Eng. Sci. Proc. 3(12), **(1982)** 519.

[30] P. Shepherd, K.K. Mallick, R.J. Green, Magnetic and structural properties of M-type barium hexaferrite prepared by co-precipitation, J. Magn. Magn. Mater. 311 **(2007)** 683-692.

[31] A. Ghasemi, A. Morisako, X. Liu, Magnetic properties of hexagonal strontium ferrite thick film synthesized by sol-gel processing using SrM nanoparticles, J. Magn. Magn. Mater. 320 (18) **(2008)** 2300– 2304.

[32] M. J. Iqbal, M .N. Ashiq, I. H. Gul, Physical, electrical and dielectric properties of Ca substituted strontium hexaferrite (SrFe12O19) nanoparticles synthesized by co-precipitation method J. Magn. Magn. Mater. 322 **(2010)** 1720–1726.

[33] H. Klug, L. Alexander, X-ray Diffraction Procedures, Wiley, New York, 79(6) (1962) 553.

[34] S. K. Chawla, R. K. Mudsainiyan, S. S. Meena, S. M. Yusuf, Sol-gel synthesis, structural and magnetic properties of nanoscale M-type barium hexaferrites $BaCo_xZr_xFe_{(12-2x)}O_{19}$. J. Magn. Magn. Mater. 350 **(2014)** 23–29.